Optoelectronic properties of coexisting $InGaZnO_4$ structures

Konstantina Iordanidou[1*] and Clas Persson[1]

[1] Centre for Materials Science and Nanotechnology, Department of Physics, University of Oslo, P.O. Box 1048 Blindern, NO-0316 Oslo, Norway

*Email: konstantina.iordanidou@smn.uio.no

Abstract

Indium gallium zinc oxides (IGZO) have been developed for thin-film transistor technologies. In this work, we analyze the fundamental properties of crystalline $InGaZnO_4$, considering all possible Ga/Zn atomic distribution patterns. Using the hybrid Hartree-Fock density functional approach, the most stable configurations are identified. The simulations reveal that the considered configurations are indirect band-gap semiconductors with highly dispersive conduction bands (CB) and very flat valence bands (VB). Thereby, the electron effective masses are light, contrary to the heavy hole effective masses. This implies a good electron mobility and suppressed hole mobility, and consequently a low off-state current that minimizes the power consumption in future $InGaZnO_4$-based transistors. Coexistence of different configurations is not an issue for $InGaZnO_4$ since they all present very similar optoelectronic properties.

Keywords: IGZO, electronic properties, optical properties, first-principles

1. Introduction

Hydrogenated amorphous silicon (a-Si:H) has been the key component of thin film transistors (TFTs), used in large-area electronic applications. However, its low mobility and poor visible-light transparency are problematic for next-generation devices, like high-performance transparent displays. To overcome such limitations, metal-oxide semiconductors (MOS) have been proposed as promising candidates to replace a-Si [1,2,3]. Among them amorphous indium-gallium-zinc-oxide (a-IGZO) has attracted intense interest [4,5,6,7]. Transparent thin film transistors (TTFTs) based on a-IGZO exhibit low off-state currents, and electron mobilities approximately one order of magnitude larger than those of a-Si:H [6].

However, despite their remarkable characteristics, such TFTs may suffer severely from instabilities under external stress. Similar to conventional TFTs, prolonged bias application can lead to the degradation of their current-voltage characteristics. By applying gate bias stress, variations of the threshold voltages, particularly parallel shifts, were observed [8]. The shifts were raised from the charge trapping process and they were logarithmically dependent on the duration of the stress [8]. In addition, light induced instabilities in the absence or along with bias stress were reported [9,10,11,12,13,14,15,16]. For instance, a-IGZO TFT using SiO_2 as gate dielectric presented large threshold voltage shift under illumination, which was increased by increasing the illumination time and decreasing the wavelength [10].

In that respect, crystalline indium-gallium-zinc-oxide (c-IGZO) may be superior from its amorphous counterpart [17]. Interestingly, sharp successfully developed and massively produced LCDs using crystalline IGZO-TFTs instead of amorphous [18]. Such LCDs can realize lower power consumption as well as higher touch panel performance compared to a-Si-TFT LCDs. Note that no significant change in the TFT characteristics after 1000-hour-operation is observed. Thus, c-IGZO-TFTs are considered to be highly reliable [17]. In this paper, we studied the structural, electronic and optical properties of c-IGZO, using first-principles calculations based on the hybrid Hartree-Fock density functional approach. We considered c-IGZO with In:Ga:Zn:O = 1:1:1:4 composition

ratio and various Ga/Zn atomic distribution patterns. The energetically favorable configurations were identified, and the energy gaps, effective masses, and dielectric constants were computed.

2. Methods and Computational details

Our first principles calculations are performed using the hybrid Hartree-Fock density functional approach, as implemented in the VASP package [19]. The electron-ion interaction is described by the projector augmented wave (PAW) method [20]. The functional proposed by Heyd, Scuseria, and Ernzerhof (HSE06) [21] is adopted here, along with the standard mixing (25% Fock exchange) and range-separation parameters. Calculations with no Fock exchange are also performed, and the generalized gradient approximation developed by Perdew, Burke, and Ernzerhof (PBE) is used for the exchange correlation functional. We model $InGaZnO_4$ using unit cells of 28 atoms in total. The unit cells have layered structures consisting of InO_2 and $(GaZn)O_2$ units. Both the volume and the atomic positions were optimized using the conjugate gradient method, with 10^{-2} eVÅ^{-1} force convergence criteria on the ionic optimization and 10^{-5} eV energy convergence criteria on the electronic minimization. The kinetic energy cutoff was set to 600 eV and the Brillouin zone was sampled by a 3×3×2 **k**-point grid for the atomic relaxations, whereas a denser grid of 6x6x4 **k**-points was used for the electronic structure and optical calculations. Convergence with respect to cutoff energy and **k**-point sampling was explicitly checked.

The optical properties are studied by means of the complex dielectric function $\varepsilon(\omega) = \varepsilon_1(\omega) + i\varepsilon_2(\omega)$ and the optical absorption coefficient $\alpha(\omega)$. The imaginary part of the dielectric function is computed from the joint density of states (JDOS) and the optical momentum matrix in the long wavelength limit [22], whereas the real part is derived from the imaginary part using the Kramers-Kronig transformation [23]. Accordingly, the absorption coefficient is directly derived from the dielectric function and the corresponding formulas are:

$$\varepsilon_2^{\alpha\beta}(\omega) = \frac{4\pi^2 e^2}{\Omega} \lim_{q\to 0} \frac{1}{q^2} \sum_{c,v,\mathbf{k}} 2w_{\mathbf{k}} \delta(E_{c\mathbf{k}} - E_{v\mathbf{k}} - \hbar\omega) \langle u_{c\mathbf{k}+e_\alpha q} | u_{v\mathbf{k}} \rangle \left\langle u_{c\mathbf{k}+e_\beta q} \middle| u_{v\mathbf{k}} \right\rangle^* \quad (1)$$

$$\varepsilon_1^{\alpha\beta}(\omega) = 1 + \frac{2}{\pi} P \int_0^\infty \frac{\varepsilon_2^{\alpha\beta}(\omega')\omega'}{\omega'^2 - \omega^2 + i\eta} \quad (2)$$

$$\alpha(\omega) = \frac{\sqrt{2}\omega}{c} \sqrt{\sqrt{\varepsilon_1(\omega)^2 + \varepsilon_2(\omega)^2} - \varepsilon_1(\omega)} \quad (3)$$

where e is the electron charge, Ω is the primitive cell volume, $w_{\mathbf{k}}$ is the weight of **k**-points, c and v refer to the valence and conduction bands, respectively, e_α and e_β are the unit vectors for the three Cartesian directions, and $u_{v\mathbf{k}}$ is the periodic part of the Bloch wave function corresponding to the eigenvalue $E_{c\mathbf{k}}$. The high-frequency dielectric constants (ε_∞) are obtained from the dielectric functions at zero frequency when the ionic contribution from the electron-optical phonon interaction is excluded, whereas the static dielectric constants (ε_0) are determined by calculating the force-constant matrices and internal strain tensors with no Fock exchange.

For the sake of comparison, calculations for the corresponding binary oxides are additionally performed. In particular, we consider wz-ZnO (space group: $P6_3mc$), β-Ga_2O_3 (space group: $C2/m$), and In_2O_3 (space group: $Ia\bar{3}$), having 4, 10, and 40 atoms in their primitive unit cells, respectively. Complementary calculations using other exchange-correlation potentials are also presented in the supplementary material.

3. 1 Structural properties and energies

c-$InGaZnO_4$ has a layered structure where In atoms occupy 6-fold coordinated sites, surrounded by an oxygen distorted octahedron, typically described as the InO_2 unit. On the other hand, Ga and Zn atoms occupy 5-fold coordinated sites, surrounded by an oxygen trigonal bipyramid, commonly referred as the $(GaZn)O_2$ unit. Ga and Zn atoms in the $(GaZn)O_2$ unit cannot be distinguished, within the X-ray resolution [24]. Thus, the Ga/Zn atomic distribution should be

theoretically investigated in order to identify the most stable structures. Figure 1 depicts all possible Ga/Zn atomic distribution patterns for the top and bottom $(GaZn)O_2$ layers. In particular, we consider six different patterns for the top $(GaZn)O_2$ layer (denoted by T_1, T_2, …, T_6) and six different patterns for the bottom $(GaZn)O_2$ layer (denoted by B_1, B_2, …, B_6), and that leads to thirty-six possible combinations. However, due to the space group symmetry only ten of these combinations are structurally non-degenerate. That is, take as an example the structures with bottom and top layers B_1T_1 and B_2T_2. By shifting the atomic positions of the B_1T_1 structure along the a-axis by 0.5a and keeping the atomic positions along the b and c-axis unshifted, one obtains the B_2T_2 structure. Table I summarizes the structural properties and total energies of the ten distinct IGZO structures. The 4-fold coordinated O atoms in the $(GaZn)O_2$ unit are bonded to either 3Ga/1Zn or 1Ga/3Zn for IGZO-I and IGZO-X, whereas they are surrounded by 2Ga/2Zn for IGZO-II and IGZO-IX. For the remaining structures, namely IGZO-III, IGZO-IV, IGZO-V, IGZO-VI, IGZO-VII, and IGZO-VIII, there are oxygens coordinated by 3Ga/1Zn, 1Ga/3Zn, as well as 2Ga/2Zn.

For all studied configurations, the In–O bond lengths in the InO_2 unit ($\delta_{\mathrm{In-O}}$), the in plane-like Ga/Zn-O bond lengths in the $(GaZn)O_2$ unit ($\delta_{\angle,\mathrm{Ga/Zn-O}}$), as well as the out of plane Ga/Zn–O bond lengths between the $(GaZn)O_2$ and InO_2 units ($\delta_{\parallel,\mathrm{Ga/Zn-O}}$) are very similar and their values are found to be $\delta_{\mathrm{In-O}} = 2.19 \pm 0.05$ Å , $\delta_{\angle,\mathrm{Ga-O}} = 1.87 \pm 0.04$ Å , $\delta_{\angle,\mathrm{Zn-O}} = 2.01 \pm 0.06$ Å , $\delta^{*}_{\parallel,\mathrm{Ga-O}} = 1.93 \pm 0.04$ Å, and $\delta^{*}_{\parallel,\mathrm{Zn-O}} = 2.01 \pm 0.04$ Å. On the other hand, the out of plane Ga/Zn-O bond lengths within the $(GaZn)O_2$ unit ($\delta_{\parallel,\mathrm{Ga/Zn-O}}$) vary depending on the structure. Note that in pairs IGZO-III, IGZO-IV, as well as IGZO-V, IGZO-VI, present nearly identical structural properties and total energies.

As observed in Table I, the most stable configuration corresponds to IGZO-VII. However, the total energies of IGZO-I, IGZO-II, and IGZO-VIII are only 0.4, 0.5, and 0.5 meV/atom larger than that of IGZO-VII. Thus, although IGZO-VII structure is the most likely one to be formed under equilibrium growth conditions, IGZO-I, IGZO-II, IGZO-VII, and IGZO-VIII can also coexist, and it is also likely to grow crystals containing different Ga/Zn atomic distributions. The least

favorable configuration corresponds to IGZO-X, but its energy is only 5.9 meV/atom larger as compared to the most stable configuration. It is worth reporting the total energies obtained from calculations with no Fock exchange. Using PBE, similar to the HSE06 results, the most favorable structures are IGZO-I, IGZO-II, IGZO-VII, and IGZO-VIII, and the least favorable structure corresponds to IGZO-X. However, IGZO-II instead of IGZO-VII is the lowest energy configuration, and the energy difference between IGZO-II and IGZO-VII is only 0.1 meV/atom. We find that the slight differences in the total energies between PBE and HSE06 calculations are mainly due to the inclusion of the Fock exchange and not due to the slight differences in the structural properties. Note that for the sake of comparison, the same parametrization scheme was used for both PBE and HSE06 calculations. As a next step, the formation enthalpies of all IGZO structures are computed using the relation $\Delta H_f = E_{InGaZnO_4} - E_{In} - E_{Ga} - E_{Zn} - 2E_{O_2}$ where E_{In}, E_{Ga}, and E_{Zn} refer to the stable solid structures of In, Ga, and Zn, respectively, whereas E_{O_2} refers to the triplet ground state structure of the O_2 molecule. For all IGZO structures, the formation enthalpies are found to be about -1.8 eV/atom, and the negative values indicate thermodynamic stability.

TABLE I. Structural properties and total energies of IGZO structures. Relative total energies are presented, taking as reference the energy of the most favorable configuration. B_1, B_2, …, B_6 and T_1, T_2, …, T_6 correspond to the different distribution patterns of Ga/Zn atoms in the bottom and top $(GaZn)O_2$ layers, respectively, whereas $\delta_{\parallel,Ga/Zn-O}$ correspond to the out of plane Ga/Zn-O bond lengths within the $(GaZn)O_2$ unit.

	Structures	a [Å]	b [Å]	c [Å]	$\delta_{\parallel,Ga-O}$ [Å]	$\delta_{\parallel,Zn-O}$ [Å]	E_{tot} [meV/atom]
IGZO-I	B_1T_1, B_2T_2, B_4T_4, B_6T_6	6.646	5.700	8.927	2.41-2.44	2.23-2.24	0.4
IGZO-II	B_1T_2, B_2T_1, B_4T_6, B_6T_4	6.641	5.725	8.854	2.18	2.35-2.37	0.5
IGZO-III	B_1T_3, B_2T_3, B_4T_5, B_6T_5	6.615	5.738	8.872	2.13-2.42	2.22-2.42	2.6
IGZO-IV	B_3T_4, B_3T_6, B_5T_1, B_5T_2	6.615	5.738	8.871	2.13-2.42	2.22-2.42	2.6
IGZO-V	B_1T_5, B_2T_5, B_4T_3, B_6T_3	6.617	5.738	8.874	2.13-2.41	2.21-2.41	3.0
IGZO-VI	B_3T_1, B_3T_2, B_5T_4, B_5T_6	6.617	5.738	8.875	2.14-2.41	2.21-2.41	3.0
IGZO-VII	B_1T_4, B_2T_6, B_4T_2, B_6T_1	6.643	5.711	8.898	2.19-2.42	2.24-2.36	0
IGZO-VIII	B_1T_6, B_2T_4, B_4T_1, B_6T_2	6.642	5.711	8.892	2.18-2.45	2.23-2.37	0.5

IGZO-IX	B_3T_3, B_5T_5	6.595	5.750	8.848	2.13	2.44	3.7
IGZO-X	B_3T_5, B_5T_3	6.590	5.781	8.850	2.30	2.24	5.9

3.2 Electronic and optical properties

Regarding the electronic properties, Fig. 2 displays the electronic band structures of IGZO structures. All studied configurations are indirect band gap semiconductors, where the conduction band (CB) minimum lies at the Γ-point, whereas the position of the valence band (VB) maximum varies depending on the structure. The band gap energies range from about 2.9 to 3.1 eV, which are in fairly good agreement with experimental observations [25]. Furthermore, Fig. 2 reveals that for all studied configurations the CB is highly dispersive, contrary to the very flat VB. Among the energetically favorable IGZO structures, IGZO-II is the compound with the flattest topmost valence band. The energy dispersion is only ~0.23 eV in the first Brillouin zone. Note that for IGZO-II, the energy difference between the indirect and direct band gap is just 0.02 eV, and for such small energy difference, the Auger effect is expected to be nearly negligible [26].

It is worth noting that calculations with the inclusion of spin orbit coupling (SOC) were also performed. Due to the low symmetry, there were no degenerate states, and no band splitting owing to this relativistic interaction. By contrast, such effect is much more pronounced in ZnO. In particular, for ZnO crystal field splits the VB into a doubly degenerate and a non-degenerate state (not counting the spin), whereas the combination of crystal field and SOC results in three doubly degenerate states.

Figure 3 depicts the total DOS as well as the atom and angular momentum projected DOS (PDOS) for IGZO-VII, and similar results are obtained for IGZO-I, IGZO-II and IGZO-VIII structures. Our PDOS calculations show that the VB can be attributed to Zn-3d and O-2p orbitals. On the other hand, the CB is formed by In-5s, Ga-4s, Zn-4s and O-2s orbitals along with the O-2p orbitals. Interestingly, a contribution of Ga-3d and In-4d states in the higher VB region is observed, and a similar d-state character has been reported for Ga_2O_3 and In_2O_3 [27,28]. To clarify the presence of the high-lying d-states, additional calculations are performed for Ga_2O_3 as an example.

By slightly decreasing the Winger-Seitz radius of the Ga atoms (and simultaneously increasing the O Winger-Seitz radius), the d-state peak near the VB maximum is reduced, whereas the main 3d-state peak at lower energies remains almost unaffected. Furthermore, including the d-electrons in the pseudopotential yields no main 3d-state peak (as expected), but still PDOS exhibits d-state character near the VB maximum (Fig. S1 in supplementary material). This analysis implies that the d-like state presence in the higher VB region shall be regarded as a consequence of the PDOS projection and a non-spherical symmetry.

Next, we compute the effective masses directly from the electronic structures using the inverse relation of the mass tensor $1/\mathrm{m}^* = \pm\partial^2\mathrm{E}(\mathbf{k})/(\hbar^2\,\partial\mathbf{k}^2)$, where + and – stand for the electrons and holes, respectively, E(**k**) is the k-resolved energy of a band, and $\hbar$ is the reduced Planck constant. In particular, the electron and hole effective masses are computed by fitting a parabola to the CB and VB extrema following the methodology in Ref. [29]. This approach yields fairly accurate values of the effective masses for traditional semiconductors as long as no anomalous dispersion occurs due to failure of the exchange-correlation function [30]; this is not expected for the adopted HSE06 functional. To avoid computational inaccuracies, a dense k-mesh is needed instead of only three k-points to represent a parabolic dispersion. In this work, we compute the energies E(**k**) for 50 k-points away from the band extrema (in specific k-directions), and for a region 10% of the first Brillouin zone. For the fitting, we have found that all considered VBs and CBs are parabolic in this 10% k-space region. Note that we follow the common approach and divide the values by the electron's rest mass m_0, i.e., the effective masses are presented in relative units.

As expected from the CB and VB dispersions, the electron effective masses are relatively light, contrary to the heavy hole effective masses. The electron effective masses are found to be highly isotropic, whereas anisotropies are observed for the hole effective masses especially for IGZO-VII structure. In particular, for IGZO-VII the hole effective masses are $6.08m_0$ and $1.68m_0$ along the RΓ and RM directions, respectively. On the other hand, the electron effective masses are found to be $0.25m_0$ and $0.26m_0$ in the ΓX and ΓZ directions, respectively, similar to the results

obtained for ZnO, Ga_2O_3, and In_2O_3 (Table SII in supplementary material). The computed values of the electron effective masses are also in fairly good agreement with previously reported theoretical calculations based on DFT [31,32]. Interestingly, all considered configurations display the same electron effective masses, whereas the hole effective masses vary depending on the structure. For instance, for IGZO-VIII the electron effective masses in the ΓX and ΓZ directions are $0.25m_0$ and $0.26m_0$, similar to the results obtained for IGZO-VII, whereas the hole effective masses are $3.54m_0$ and $3.66m_0$ along the RΓ and RM directions, respectively.

Overall, our effective mass calculations confirm that $InGaZnO_4$ is a promising candidate for replacing Si as a channel material in future transistors. In particular, the light electron effective mass results in high electron mobility. Accordingly, the heavy hole effective mass leads to low hole mobility, and subsequently to low off-state current, minimizing the power consumption in $InGaZnO_4$-based transistors. As a last step, c-$InGaZnO_4$ structure consisting of pure GaO and ZnO layers is considered. Such configuration is isostructural with $YbFe_2O_4$ which belongs to $R\bar{3}m$ space group. However, the substitution of two Fe atoms by one Ga and one Zn reduces the symmetry, leading to the $R3m$ space group [33]. Upon relaxation, Ga and Zn atoms are no longer in equivalent positions, and the total energy is much higher compared to those of $InGaZnO_4$ structures with mixed $(GaZn)O_2$ layers.

Regarding the optical properties, the dielectric function $\varepsilon(\omega) = \varepsilon_1(\omega) + i\varepsilon_2(\omega)$ describes the electronic response to a charge distribution change, and such response is crucial for defining the electronic screening near structural perturbations like defects and dopants. Figure 4 depicts the real $\varepsilon_1(\omega)$ and imaginary $\varepsilon_2(\omega)$ parts of the dielectric function, as well as the absorption coefficient, of only IGZO-VII, since IGZO-I, IGZO-II, and IGZO-VIII have very similar spectra (Fig. S2 in supplementary material). The static and high-frequency dielectric constants, for the most favorable structures, are presented in Table II. The optical onsets occur at photon energies $\hbar\omega = E_g^d$. In the range of $0 \leq \hbar\omega \leq \sim 4$ eV, the real part of the dielectric function increases monotonically as a function of the energy. The mid-gap values are found to be fairly isotropic $\varepsilon_1^{xx}(\omega = E_g/2\hbar) =$

$\varepsilon_1^{yy}(\omega = E_g/2\hbar) = 3.5$ and $\varepsilon_1^{zz}(\omega = E_g/2\hbar) = 3.4$ for all configurations, and the corresponding values at the band gap energy are $\varepsilon_1^{xx}(\omega = E_g/\hbar) = \varepsilon_1^{yy}(\omega = E_g/\hbar) = \varepsilon_1^{zz}(\omega = E_g/\hbar) = 3.7$, 3.8, 3.7, and 3.7 for IGZO-I, IGZO-II, IGZO-VII, and IGZO-VIII structures, respectively. For the considered configurations, the high-frequency dielectric constants are ~3.4, whereas the in plane static dielectric constants are ~ 8.3, i.e., similar to the results for ZnO [34]. Notably, a strong anisotropy is observed for the static dielectric constants, and the computed values along the z direction are 22.7, 17.6, 20.5, and 19.8 for IGZO-I, IGZO-II, IGZO-VII, and IGZO-VIII, respectively, i.e., c-$InGaZnO_4$ is a high-κ-like material in this direction. The average static dielectric constant ranges from about 11 to 13 for the considered structures, which is in fairly good agreement with experimental observations for a-$InGaZnO_4$ [35].

TABLE II. Electronic and optical properties of the most favorable IGZO structures, namely IGZO-I, IGZO-II, IGZO-VII, and IGZO-VIII. E_g and E_g^d correspond to the indirect and direct band gap energies, respectively, whereas ΔW_v corresponds to the energy width of the uppermost VB. For the electron effective masses (m_e) the considered directions are indicated in parenthesis. The static (ε_0) and high frequency (ε_∞) dielectric constants are presented for the *x*- and *z*-directions, whereas the component in the *y*-direction is very similar to that of the *x*-direction.

	IGZO-I	IGZO-II	IGZO-VII	IGZO-VIII
E_g [eV]	2.94	3.06	2.94	2.90
E_g^d [eV]	3.13	3.08	3.05	3.11
ΔW_V [eV]	0.34	0.23	0.37	0.35
$m_e[m_0]$	0.25 (ΓX)	0.25 (ΓX)	0.25 (ΓX)	0.25 (ΓX)
$m_e[m_0]$	0.26 (ΓZ)	0.26 (ΓZ)	0.26 (ΓZ)	0.26 (ΓZ)
ε_∞^{xx}	3.4	3.4	3.4	3.4
ε_∞^{zz}	3.3	3.4	3.3	3.3
ε_0^{xx}	8.3	8.3	8.3	8.3
ε_0^{zz}	22.7	17.6	20.5	19.8

4. Conclusions

To conclude, we have studied the structural, electronic, and optical properties of crystalline $InGaZnO_4$ using atomistic first-principles calculations. Since Ga/Zn atoms cannot be distinguished within the X-ray resolution, we considered all possible Ga/Zn atomic distribution patterns and we identified the most stable structures by computing their total energies. Specifically, we conclude that coexistence of different configurations is not an issue for c-IGZO since they all present very similar optoelectronic properties, with indirect band gaps, highly dispersive CBs and very flat VBs. The electron effective masses are found to be light contrary to the heavier hole effective masses. The high-frequency dielectric constants are found to be isotropic (~3.4), whereas the static dielectric constants exhibit strong anisotropy with one high-κ component (~8 in-plane whereas ~20 in the z-direction). For all considered configurations, the absorption spectra are very similar, and overall c-IGZO present promising optoelectronic properties.

Acknowledgements

This work has been financially supported by the Research Council of Norway (ToppForsk project: 251131). We acknowledge access to HPC resources Abel and Fram in Norway with allocation provided through NOTUR.

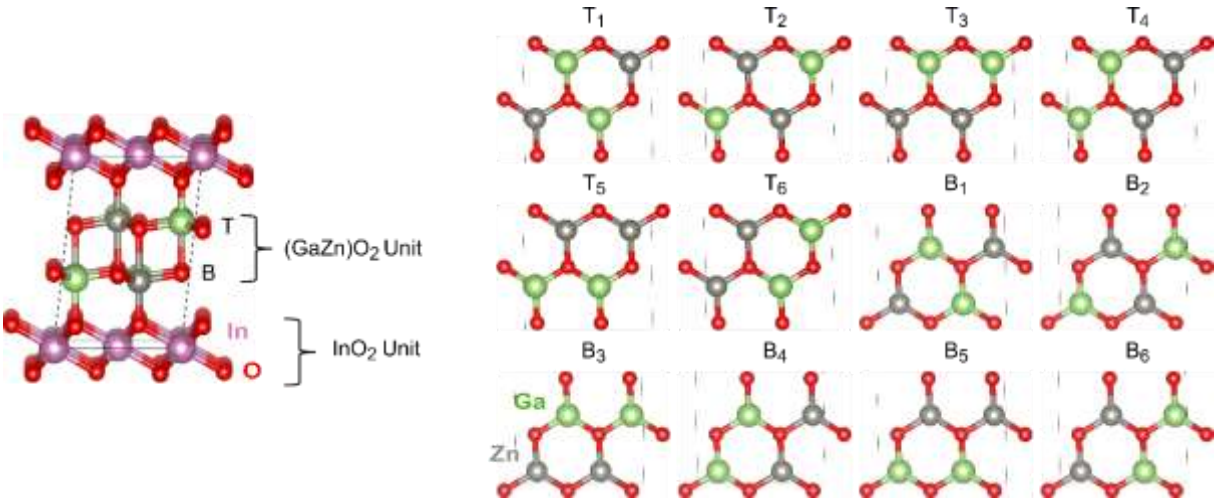

FIG. 1. c-IGZO unit cell consisting of InO_2 and $(GaZn)O_2$ units, as well as different distribution patterns of Ga/Zn atoms in the top (T_1, T_2, …, T_6) and bottom (B_1, B_2, …, B_6) $(GaZn)O_2$ layers. Purple, green, gray and red spheres correspond to In, Ga, Zn and O atoms, respectively.

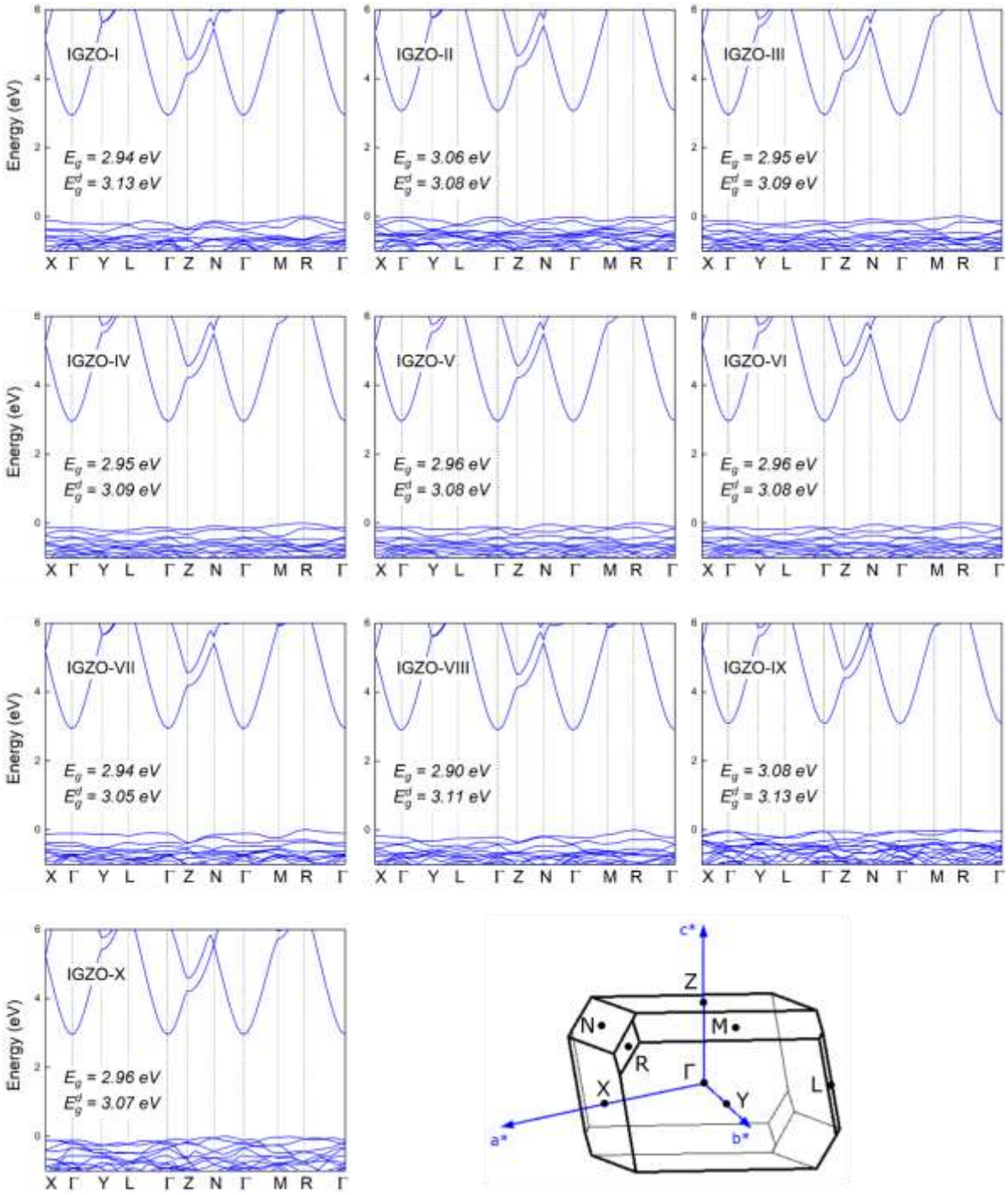

FIG. 2. Electronic band structures of IGZO structures and the corresponding Brillouin zone. The energies refer to the VB maximum. E_g and E_g^d denote the indirect and Γ-point direct gaps, respectively. The high-symmetry **k**-points are: X (0.5, 0, 0), Γ (0, 0, 0), Y (0, 0.5, 0), L (-0.5, 0.5, 0), Z (0, 0, 0.5), N (0.5, 0, 0.5), M (0, 0.5, 0.5), and R (0.5, 0.5, 0.5).

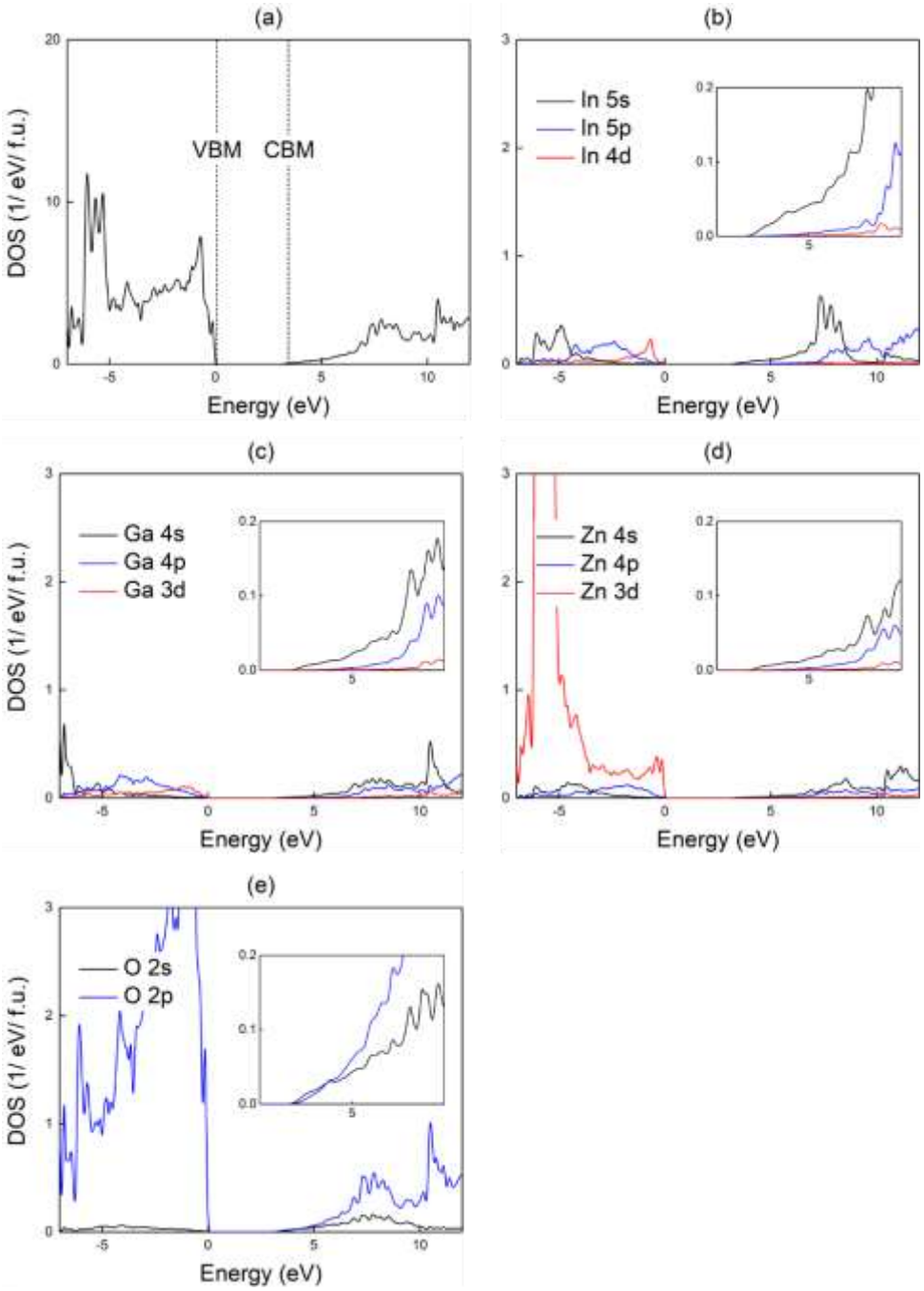

FIG. 3. Total (a) and projected (b-e) DOS per formula unit (f.u.) of IGZO-VII structure. In the total DOS, the positions of the VB maximum (VBM) and CB minimum (CBM) are denoted by dashed lines. The spectra include a 0.05 eV Lorentzian broadening, and the insets show a close-up at the conduction region. IGZO-I, IGZO-II and IGZO-VIII structures present very similar DOS compared to IGZO-VII.

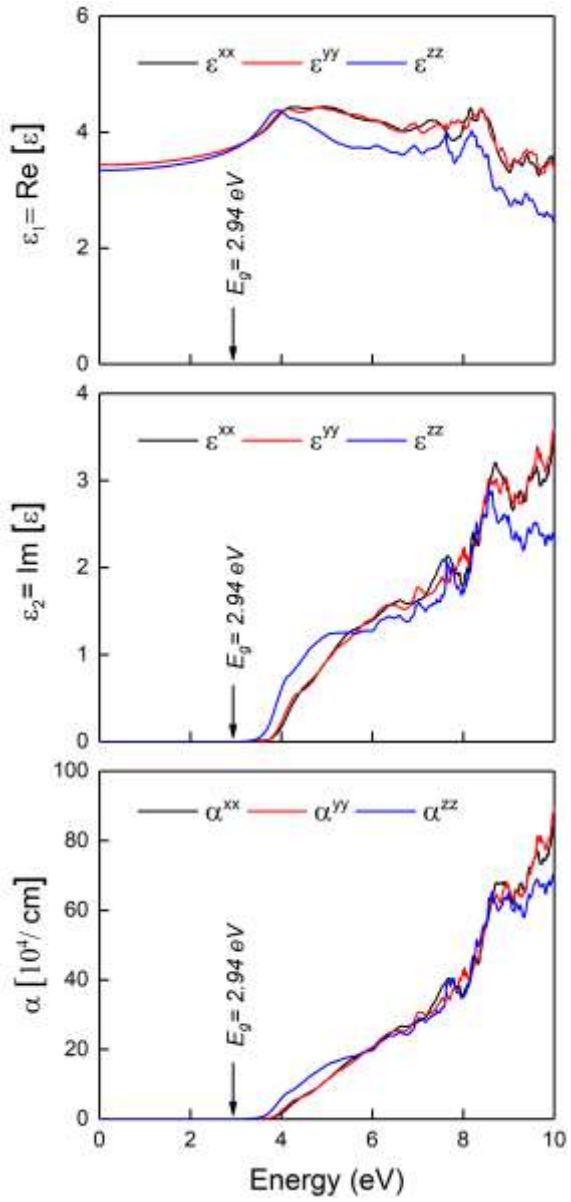

FIG. 4. The real and imaginary parts of the dielectric function $\varepsilon(\omega) = \varepsilon_1(\omega) + i\varepsilon_2(\omega)$ of IGZO-VII, as well as the absorption coefficient $\alpha(\omega)$.

References

[1] M. G. Kim, M. G. Kanatzidis, A. Facchetti, and T. J. Marks, Low-temperature fabrication of high-performance metal oxide thin-film electronics via combustion processing, Nat. Mater. 10, 382 (2011).

[2] S. Y. Han, G. S. Herman, and C. H. Chang, Low-temperature, high-performance, solution-processed indium oxide thin-film transistors, J. Am. Chem. Soc. 133, 5166 (2011).

[3] K. K. Banger, Y. Yamashita, K. Mori, R. L. Peterson, T. Leedham, J. Rickard, and H. Sirringhaus, Low-temperature, high-performance solution-processed metal oxide thin-film transistors formed by a 'sol–gel on chip' process, Nat. Mater. 10, 45 (2011).

[4] T. Kamiya, and H. Hosono, Material characteristics and applications of transparent amorphous oxide semiconductors, NPG Asia Mater. 2, 15 (2010).

[5] H. Yabuta, M. Sano, K. Abe, T. Aiba, T. Den, H. Kumomi, K. Nomura, T. Kamiya, and H. Hosono, High-mobility thin-film transistor with amorphous channel fabricated by room temperature rf-magnetron sputtering, Appl. Phys. Lett. 89, 112123 (2006).

[6] K. Nomura, H. Ohta, A. Takagi, T. Kamiya, M. Hirano, and H. Hosono, Room-temperature fabrication of transparent flexible thin-film transistors using amorphous oxide semiconductors, Nature 432, 488 (2004).

[7] H. Hosono, Ionic amorphous oxide semiconductors: Material design, carrier transport, and device application, J. Non-Cryst. Solids 352, 851 (2006).

[8] A. Suresh, and J. F. Muth, Bias stress stability of indium gallium zinc oxide channel based transparent thin film transistors, Appl. Phys. Lett. 92, 033502 (2008).

[9] D. P. Gosain, and T. Tanaka, Instability of amorphous indium gallium zinc oxide thin film transistors under light illumination, Jpn. J. Appl. Phys. 48, 03B018 (2009).

[10] M. D. H. Chowdhury, P. Migliorato, and J. Jang, Light induced instabilities in amorphous indium–gallium–zinc–oxide thin-film transistors, Appl. Phys. Lett. 97, 173506 (2010).

[11] J. Chen, J. Xu, M. Wang, and L. Cai, Photo-induced instability and temperature dependence of amorphous In-Ga-Zn-O thin film transistors, Proceedings of the 20th IEEE International Symposium on the Physical and Failure Analysis of Integrated Circuits (IPFA), 690 (2013).

[12] Y. C. Tsao, T. C. Chang, S. P. Huang, Y. L. Tsai, M. C. Tai, H. Y. Tu, H. C. Chen, J. W. Huang, and S. Zhang, Effects of Ultraviolet Light on the Dual-Sweep I–V Curve of a-$InGaZnO_4$ Thin-Film Transistor. IEEE Trans. Electron Devices, 66, 1772 (2019).

[13] W. T. Chen, H. W. Hsueh, H. W. Zan, and C. C. Tsai, Light-enhanced bias stress effect on amorphous In-Ga-Zn-O thin-film transistor with lights of varying colors, Electrochem. Solid-State Lett. 14, H297 (2011).

[14] H. Oh, S. M. Yoon, M. K. Ryu, C. S. Hwang, S. Yang, and S. H. K. Park, Transition of dominant instability mechanism depending on negative gate bias under illumination in amorphous In-Ga-Zn-O thin film transistor, Appl. Phys. Lett. 98, 033504 (2011).
[15] T.C. Chen, T.C. Chang, C.T. Tsai, T.Y. Hsieh, S.C. Chen, C.S. Lin, M.C. Hung, C.H. Tu, J.J. Chang, and P.L. Chen, Behaviors of InGaZnO thin film transistor under illuminated positive gate-bias stress, Appl. Phys. Lett. 97, 112104 (2010).
[16] H. Oh, S. M. Yoon, M. K. Ryu, C. S. Hwang, S. Yang, and S. H. K. Park, Photon-accelerated negative bias instability involving subgap states creation in amorphous In–Ga–Zn–O thin film transistor, Appl. Phys. Lett. 97, 183502 (2010).
[17] K. Park, H.W. Park, H.S. Shin, J. Bae, K.S. Park, I. Kang, K.B. Chung, and J.Y. Kwon, Reliability of crystalline indium–gallium–zinc-oxide thin-film transistors under bias stress with light illumination, IEEE Trans. Electron Devices 62, 2900 (2015).
[18] Y. Kataoka, H. Imai, Y. Nakata, T. Daitoh, T. M. N. Kimura, T. Nakano, Y. Mizuno, T. Oketani, M. Takahashi, M. Tsubuku, H. Miyake, T.I.Y. Hirakata, J. Koyama, S. Yamazaki, J. Koezuka, K. Okazaki, Development of IGZO-TFT and creation of new devices using IGZO-TFT, Dig. Tech. Pap. - SID Int. Symp. 44, 771 (2013).
[19] G. Kresse, and J. Furthmüller, Efficiency of ab-initio total energy calculations for metals and semiconductors using a plane-wave basis set, Comput. Mater. Sci. 6, 15 (1996).
[20] P. E. Blöchl, Projector augmented-wave method, Phys. Rev. B: Condens. Matter Mater. Phys. 50, 1795 (1994).
[21] J. Heyd, G. E. Scuseria, and M. Ernzerhof, Hybrid functionals based on a screened Coulomb potential, J. Chem. Phys. 118, 8207 (2003).
[22] M. Gajdoš, K. Hummer, G. Kresse, J. Furthmüller, and F. Bechstedt, Linear optical properties in the projector-augmented wave methodology, Phys. Rev. B 73, 045112 (2006).
[23] V. Lucarini, J.J. Saarinen, K.E. Peiponen, and E.M. Vartiainen, Kramers-Kronig relations in optical materials research, Springer Science & Business Media, Berlin (2005).
[24] M. Nespolo, A. Sato, T. Osawa, and H. Ohashi, Synthesis, Crystal Structure, and Charge Distribution of $InGaZnO_4$. X-ray Diffraction Study of 20kb Single Crystal and 50kb Twin by Reticular Merohedry, Cryst. Res. Technol. 35, 151 (2000).
[25] M. Orita, M. Takeuchi, H. Sakai, and H. Tanji, New transparent conductive oxides with $YbFe_2O_4$ structure, Jpn. J. Appl. Phys. 34, L1550 (1995).
[26] R. Chen, and C. Persson, High absorption coefficients of the $CuSb(Se, Te)_2$ and $CuBi(S, Se)_2$ alloys enable high-efficient 100 nm thin-film photovoltaics, EPJ Photovoltaics 8, 85504 (2017).
[27] C. Tang, J. Sun, N. Lin, Z. Jia, W. Mu, X. Tao, and X. Zhao, Electronic structure and optical

property of metal-doped Ga_2O_3: a first principles study, RSC Adv. 6, 78322 (2016).
[28] P. D. C. King, T. D. Veal, F. Fuchs, Ch. Y. Wang, D. J. Payne, A. Bourlange, H. Zhang, G. R. Bell, V. Cimalla, O. Ambacher, R. G. Egdell, F. Bechstedt, and C. F. McConville, Band gap, electronic structure, and surface electron accumulation of cubic and rhombohedral In_2O_3, Phys. Rev. B 79, 205211 (2009).
[29] R. Chen, and C. Persson, Parameterization of $CuIn_{1-x}Ga_xSe_2$ (x = 0, 0.5, and 1) energy bands. Thin solid films, 519, 7503 (2011).
[30] C. Persson, and S. Mirbt, Improved electronic structure and optical properties of sp-hybridized semiconductors using LDA+U, Br. J. Phys. 36, 286 (2006).
[31] N. Kimizuka and S. Yamazaki, Physics and Technology of Crystalline Oxide Semiconductor CAAC-IGZO : Fundamentals (Wiley, 2017).
[32] J.E. Medvedeva, Averaging of the electron effective mass in multicomponent transparent conducting oxides, EPL 78, 57004 (2007).
[33] A. D. J. de Meux, G. Pourtois, J. Genoe, and P. Heremans, Comparison of the electronic structure of amorphous versus crystalline indium gallium zinc oxide semiconductor: structure, tail states and strain effects, J. Phys. D: Appl. Phys. 48, 435104 (2015).
[34] O. Madelung, Semiconductors: Data Handbook, 3rd ed. (Springer, Berlin, 2004).
[35] J. Zhang, Y. Li, B. Zhang, H. Wang, Q. Xin, A. Song, Flexible indium–gallium–zinc–oxide Schottky diode operating beyond 2.45 GHz, Nat. Commun. 6, 7561 (2015).